

Fatigue Assessment of Steel Riveted Railway Bridges: Full-Scale Tests and Analytical Approach.

Elisa Bertolesi ^{a*}, Manuel Buitrago ^b, Jose M. Adam ^{b, c}, Pedro A. Calderón ^{b, c}

^a Department of Civil and Environmental Engineering, Brunel University London, UB8 3PH Uxbridge, UK

^b ICITECH, Universitat Politècnica de València, Camino de Vera s/n, 46022 Valencia, Spain

^c CALSENS, Camino de Vera s/n, 46022 Valencia, Spain

* Corresponding author: elisa.bertolesi@brunel.ac.uk

Keywords: Fatigue, Structural Health Monitoring, Steel bridges, Truss structures, Full-scale tests.

Abstract

This paper describes a double experimental and analytical study of the fatigue behaviour of the Quisi and Ferrandet Bridges, twin 170 m long steel railway bridges constructed between 1913 and 1915 with typical Pratt truss structures and riveted connections. These bridges are part of the Spanish national railway network connecting the towns of Alicante and Denia, one of the key networks in the Valencia Region (Spain). The experimental laboratory investigation involved fatigue testing in one of the ICITECH laboratories at the *Universitat Politècnica de València* of: (i) a full-scale bridge span and (ii) an upper cross beam from the Ferrandet bridge. During the tests, Linear Variable Displacement Transducers (LVDTs) and Strain Gauge (SG) sensors were used to capture the possible nucleation and propagation of fatigue cracks. Fatigue test carried out on the cross beam identified: (i) **fatigue life of the critical detail**, (ii) fatigue hot-spots along the cross beam and (iii) strain redistribution along the riveted element during crack growth. The experimental results from the full-scale bridge were adopted to calibrate an elastic numerical model of the whole structure, which was in turn used to estimate the Quisi Bridge's remaining fatigue life. The definition of the class of detail and remaining fatigue life were calculated by the S-N curves method, according to Eurocode 3, considering the available information on the bridges' loading histories.

30 **1. Introduction**

31 Most steel bridges designed between the early 19th century and the mid-20th century were
32 built of structural steel with riveted joints. The fatigue behaviour of riveted joints has become a
33 topic of interest due to the large number of bridges of this type still in service despite the heavy
34 traffic volumes they have sustained over the years. A fact that deserves special mention is that
35 more than 60% of the railway bridges in Europe are over 50 years old and more than 30% are
36 over 100 years old [1]-[9]. Most of these bridges were built prior to standardization
37 [10][11][12][13] and the widespread use of design codes, and now are subjected to higher loads
38 and speeds than those for which they were originally designed. Many therefore require
39 maintenance and in some cases need to be partially or completely replaced.

40 Due to the large number of riveted steel railway bridges in Europe, replacing all these structures
41 will be extremely costly and virtually impossible unless phased over several decades [7]. The
42 riveted connection construction technique has been one of the most durable techniques in the
43 history of steel bridges and was the preferred system until the 20th century [5][6]. In spite of
44 this, the damage statistics of various steel structures clearly demonstrate that steel bridges are
45 38% more likely to fail due to fatigue crack propagation [1]. Several studies [2][4][8] indicate
46 that old riveted bridges suffer from a combination of multiple aspects, including construction
47 material characteristics and degradation, while [2] points out that old riveted bridges were
48 mainly constructed using puddle iron and mid-low carbon steel. The combination of
49 heterogeneous material and slag with low C and Si contents favour degradation processes and
50 reduce the steel's chemical and mechanical resistance to microstructural damage and promote
51 the nucleation of fatigue cracks. These findings also apply to other types of steel bridges
52 constructed in the same era.

53 Microstructural damage is likely to affect the structural behaviour of steel bridges only at an
54 advanced state of crack propagation. The observations of studies adopting multiple approaches
55 highlighted their high structural redundancy as a common feature. This means that the failure of
56 a component generally does not lead to the gradual collapse of the entire structure, since a crack
57 in a riveted girder will most likely remain within the cracked component. In this situation the
58 rivets help the compartmentation of the damage in the cracked girder and prevent it from
59 spreading to other elements. However, after the failure of one element and the distribution of
60 the loads to the remaining components, a progressive failure can start or there may even be a
61 new fatigue failure due to the higher cyclic loads they receive. In-field monitoring of steel
62 railways bridges [14]-[17] is therefore of paramount importance in understanding the actual
63 state of steel structures subjected to cyclic loads.

64 The authors of [16] pointed out that fatigue damage is expected to occur in primary elements,
65 mostly in stringers and cross beams, which directly bear the cyclic loads. Similar findings
66 emerged in [18]-[20], when the authors analysed the fatigue behaviour of riveted connections.
67 Advanced numerical studies later confirmed by experimental tests [21] revealed that the angle
68 fillet and the rivet head-to-shank junction and holes are fatigue-starting hot-spots. The authors
69 of [18] demonstrated by means of several parametric FE analyses that defects can affect the
70 fatigue behaviour of riveted connections in the presence of: (i) clearance between the rivet
71 shank and rivet hole and (ii) the loss of a rivet. The authors in [22] analysed the behaviour of
72 stringer-to-floor beam connections in old riveted bridges and underlined that primary elements
73 are the most prone to experience fatigue failures because they are usually short in length and
74 accumulate large stress fluctuations. The fatigue tests performed by the authors also revealed
75 that riveted connections performed better than expected, assuming detail class 71, thus,
76 confirming that it is a safer assumption in the absence of experimental data [22]. They also
77 found that **the state of stress** is strongly influenced by the connection quality and thus its end-
78 fixity plays a crucial role.

79 Considering the level of skill required to produce riveted connections and the absence of
80 standardized quality controls, it is not surprising that the authors detected high uncertainty
81 related to the determination of rivet fatigue strength. Among the experimental works carried
82 out on riveted elements, it is worth mentioning the investigations carried out in [23][24]. In
83 [23] the authors performed a wide experimental and analytical investigation on riveted railway
84 bridge girders and subjected them to full-scale bending tests. The lab tests confirmed that the
85 critical point in the bridge was the riveted connections of the shear-diaphragms directly
86 carrying the loads. Fatigue failure also originated in rivet shanks and resulted in their head loss.
87 Finally, a detail category of 117 was suggested. In [24] the authors experimentally analysed the
88 behaviour of a 12.4 m long railway bridge. In agreement with [22] and [23], Pipinato et al.
89 identified the riveted connections of the shear diaphragms carrying the rails as the bridge's
90 fatigue hot-spot, mainly in the rivet shanks. The analytical studies confirmed that a detail class
91 of 100 should be preferred in case of failure triggered by **tangential stresses (shear stresses)**.
92 This finding is partially in agreement with Eurocode 3 recommendations that suggest detail
93 classes 80 and 100 should be adopted.

94 From a structural point of view, few studies [25][26] in the literature deal with the experimental
95 fatigue testing of full-scale riveted bridges or subassemblies due to the huge financial and
96 operational implications. The aim of the present study was to enrich the broader scenario of
97 experimental fatigue studies of riveted elements with a double experimental and analytical
98 study dealing with: (i) a full-scale span of a riveted steel railway bridge after more than 100

99 years of operational service and (ii) a full-scale localized fatigue test of a cross beam. The results
100 obtained from the two lab tests were coupled with load tests on bridges, Linear-Static Finite-
101 Element Analysis (LSFEAs) and the current recommendations to define an integrated multi-field
102 analytical method for predicting the residual fatigue life of steel bridges. The proposed
103 approach could be extended to other bridges on the basis of: (i) real loading tests and (ii)
104 numerical simulations, assuming detail categories 71 and 100, according to whether the
105 expected failure mechanism is normal or tangential. This method was also applied in this work
106 to the Quisi Bridge, which is still in service.

107 The paper is organized as follows: After this Introduction, Section 2 describes the bridge
108 geometry, while Section 3 describes the method used in the study. Sections 4 and 5 report the
109 results obtained from both studies and Section 6 discusses the analytical approach adopted to
110 estimate the detail class and the bridge's residual fatigue life. Section 7 summarizes the most
111 important findings obtained and outlines future work.

112 2. Geometrical description of the Quisi and Ferrandet Bridges

113 These Pratt truss bridges are part of the Spanish national railway network connecting the towns
114 of Alicante and Denia and were constructed between 1913 and 1915. As can be seen in **Figure**
115 **1**, the Quisi Bridge is approximately 170 m long and is composed of 6 spans with lengths
116 varying between 21 and 42 m resting on two lateral abutments (LA 1 and 2) and five steel truss
117 columns (P1, P2, P3, P4 and P5) of different heights fixed to ashlar foundations. The two central
118 spans form a continuous hyperstatic beam (spans 3 & 4), while the lateral spans 1, 2, 5 and 6
119 were constructed as isostatic elements. The span nomenclature and main geometrical details
120 are also reported in **Figure 1** and **Figure 2**.

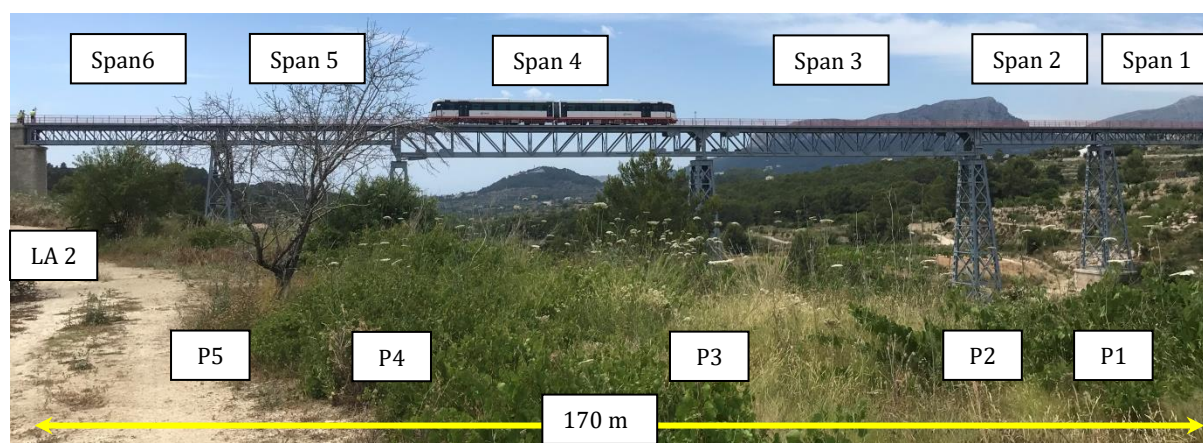


Figure 1: Quisi bridge geometry and span nomenclature.

121 After more than 100 years in service and due to the general increase in rail traffic, the railway
122 company activated different restoration strategies for steel bridges, one of which involved

Revised version, modifications highlighted in color **YELLOW**

123 replacing the Ferrandet Bridge by a completely new structure. This gave us a unique
124 opportunity to move one of its spans, with the same geometry as spans 2 and 5 of the Quisi
125 Bridge, to the ICITECH laboratories at the *Universitat Politècnica de València* (Valencia, Spain),
126 where it was tested under fatigue loads. The results obtained can be extended to other similar
127 railway bridges (like the Quisi Bridge, **Figure 2**), with the same geometry.

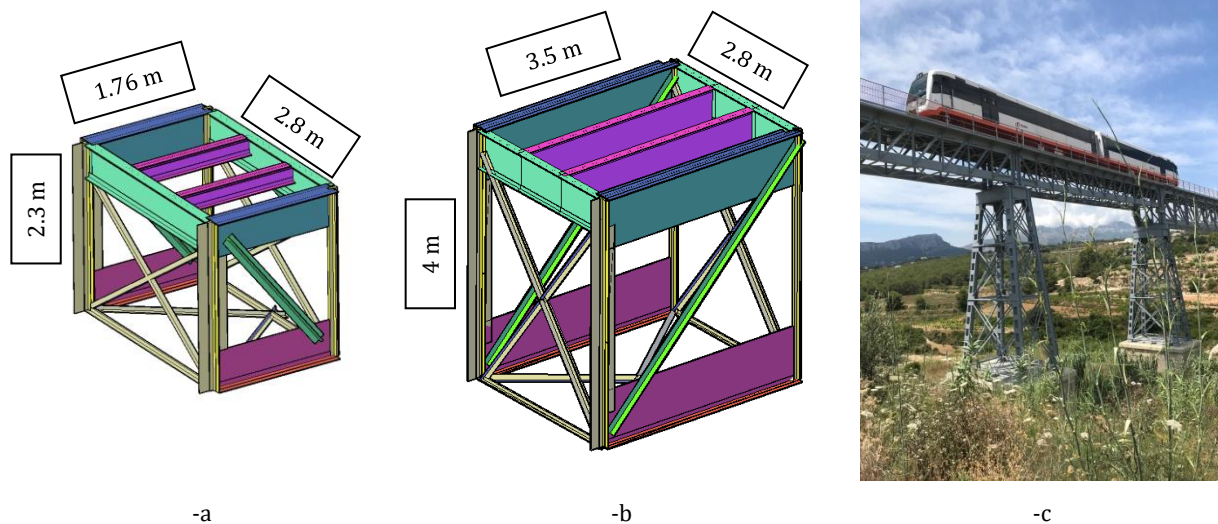


Figure 2: Quisi bridge: geometry of the isostatic (-a) and iperstatic (-b) modules and (-c) 3D view of piers 4 and 5.

128 3. Experimental investigation

129 3.1 Methodology

130 The study was organized into two parts: a laboratory study and an analytical assessment. The
131 experimental results were used to validate the current recommendations proposed by
132 Eurocode 3 and extend our knowledge of fatigue failures in old riveted steel elements. It was
133 considered of paramount importance to test riveted bridge structures after years of operational
134 service and environmental degradation. Since fatigue tests on full-scale bridges under
135 controlled laboratory conditions have obvious technical limitations, it was decided to carry out
136 a double experimental investigation on two different scales. One of the lab tests was on an
137 upper cross beam subjected to railway load cycles and thus vulnerable to fatigue damage. The
138 second, and more ambitious, lab test was applying cyclic loads to a full-scale isostatic bridge
139 span.

140 The first test identified the following data: (i) maximum number of cycles before fatigue failure,
141 (ii) identification of fatigue hot-spots inside the element, (iii) the precision, position and utility
142 of the different SG and LVDT sensors and (iv) crack growth rates. The information from (i)
143 allowed us to define the detail class by adopting the S-N curves method proposed in
144 [10][11][13][26] (see below). The data provided by (ii), (iii) and (iv) identified effective fatigue-

145 crack monitoring strategies. The results from the second investigation were used to calibrate a
 146 Finite Element numerical model for the analytical assessment. The overall findings were: (i) the
 147 identification of the elements most vulnerable to fatigue failure, and (ii) the expected
 148 operational life up to fatigue failure.

149 **3.2 Preliminary assessment of materials**

150 The following tests were performed on different samples from the bridges: (i) tensile tests
 151 according to EN ISO 6892-1 [27] (ii) the Charpy impact test according to EN ISO 148-1 [28] and
 152 (iii) mineralogical and chemical tests. The mechanical and impact test results are summarized in
 153 **Table 1** and **Table 2**. All the tested samples showed consistent results in terms of both yielding
 154 and ultimate strengths, while the impact results were widely scattered. The good quality of the
 155 steel comparable with that of current steel can be seen in the results in Table 1.

Table 1: Quisi and Ferrandet bridges: tensile test results.

Sample	Yielding strength	Ultimate strength	Elongation [%]
	[MPa]	[MPa]	
Quisi	271	399	32
Ferrandet	299	325	36

156

Table 2: Quisi and Ferrandet bridges: Charpy impact test results (Joule).

Sample	Temperature [°C]	
	0	20
Quisi	32	64
Ferrandet	18	34

157 The chemical results are summarized in **Table 3** for different types of samples (rivet, plate and
 158 profile). According to [2], the brittle nature of old riveted bridges is associated with the
 159 presence of impurities and low C and Si content steel (<0.1% and 0.03%, respectively). The
 160 Ferrandet Bridge clearly shows these features while the Quisi Bridge has higher C and Si
 161 contents.

Table 3: Chemical test results of Quisi and Ferrandet Bridges (%).

Bridge	Sample	C	Si	Mn	P	S	Cr	Ni	Mo
Quisi	Rivet	0.193	0.018	0.492	0.060	>0.130	-	-	-
Ferrandet		0.037	0.036	0.33	0.048	0.063	-	-	-
Quisi	Plate	0.139	0.108	0.520	0.079	0.072	-	-	-
Ferrandet		0.046	<0.017	0.336	0.063	0.089	-	-	-
Quisi	Profile	0.139	0.105	0.510	0.066	0.071	-	-	-
Ferrandet		0.042	<0.017	0.346	0.041	0.050	-	-	-

162

163

164 4. Riveted cross beam element

165 4.1 Fatigue load protocols and experimental set-up

166 The geometry of the tested element is shown in **Figure 3-a**, while **Figure 3-b** depicts the
167 experimental set-up adopted.

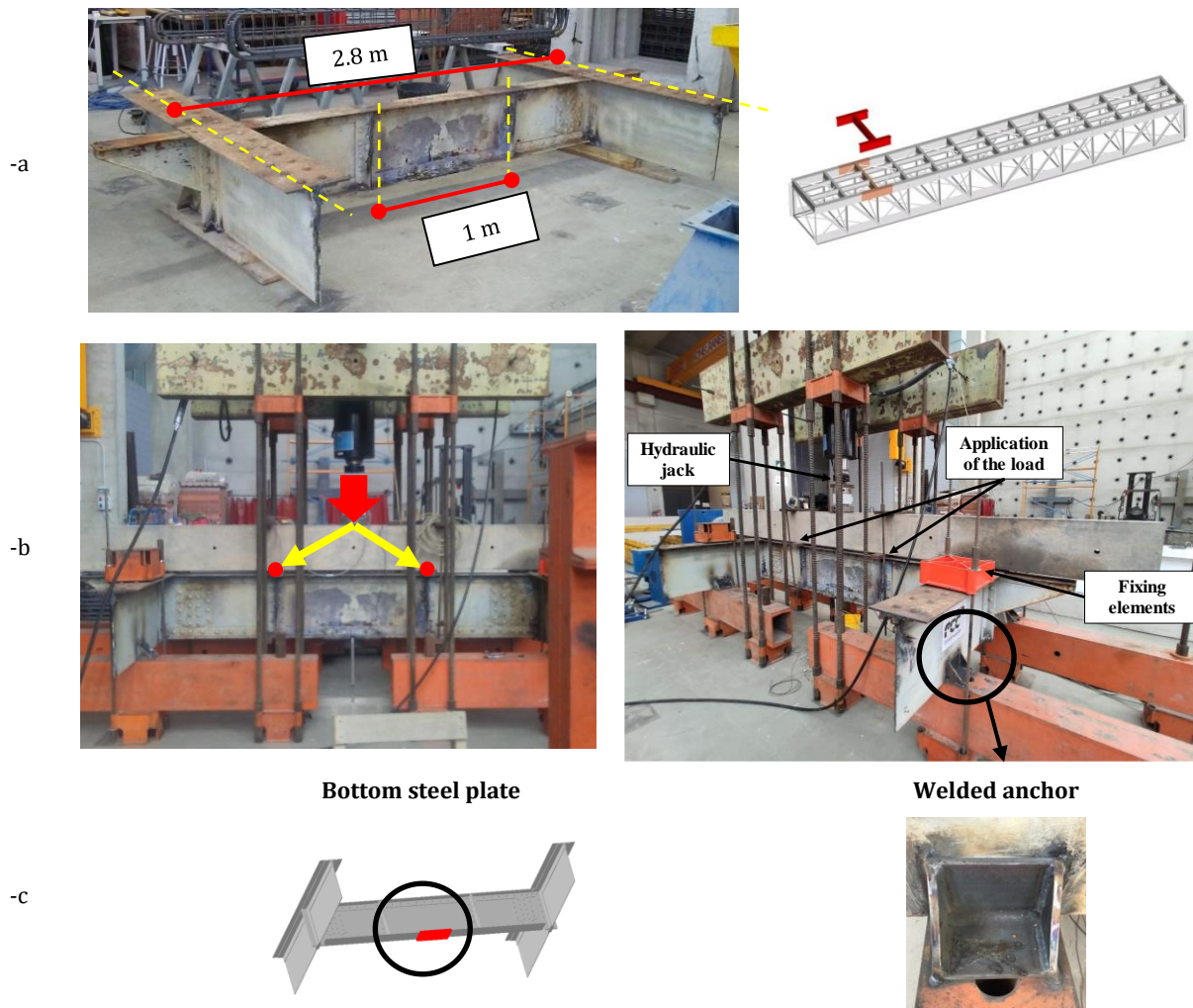


Figure 3: Geometry of the riveted truss beam tested (-a), experimental set-up (-b) and details of the beam and welded anchors (-c).

168 The experimental set-up comprised the application of a 0.55 Hz frequency cyclic load
169 (maximum speed of the hydraulic jack) ranging from 50 to 650 kN, redistributed at two points
170 by a stiff beam designed to simulate load transfers in real traffic scenarios. The loading points
171 were in fact under the railway tracks. The load range and frequency were determined in order
172 to exploit the maximum capability of the hydraulic jack used during the investigation. To this
173 scope, the experimental design stress range was designed to reasonably minimize the number

174 of cycles (using S-N curve method) whilst preventing the structures to experience any plastic
 175 deformation that could trigger (or anticipate) the formation of fatigue cracks. The same strategy
 176 was used when designing the experimental test on the full-scale span bridge. Lateral restraints
 177 play a crucial role in the stress state of the riveted beam when subjected to cyclic loads, when
 178 the riveted beam is mainly subjected to bending transmitted to the lateral chords by the riveted
 179 connections. The riveted beam was firmly anchored to the reaction floor by four lateral welded
 180 anchors positioned so that they did not introduce additional stiffness to the lateral restraints. A
 181 detail of the anchorage can be seen in **Figure 3-b-c**.

Table 4: Description of sensor positions

Sensor	Position	Sensor	Position
SG 1	Centre, lateral bottom part of the web	LVDT 1	Mid-span
SG 2	Centre, mid lower flange	LVDT 2	Lateral riveted connection
SG 3	Centre, mid lateral lower flange		
SG 4	Centre, mid upper flange		

182 The fatigue behaviour of the riveted element was monitored by four strain gauges (SG) and two
 183 Linear Variable Displacement Transducers (LVDT). **Figure 4** shows the sensor network, while
 184 **Table 4** gives their positions. Fatigue cracks can be initiated by abrupt local changes in the cross
 185 section, such as by the presence of an additional steel plate anchored to the beam bottom
 186 flanges (see **Figure 3**). One LVDT was positioned below the tested element to monitor vertical
 187 deflections and another to evaluate possible relative movements between rivet head and the
 188 lateral profile indicating a possible weak point of the cross beam.

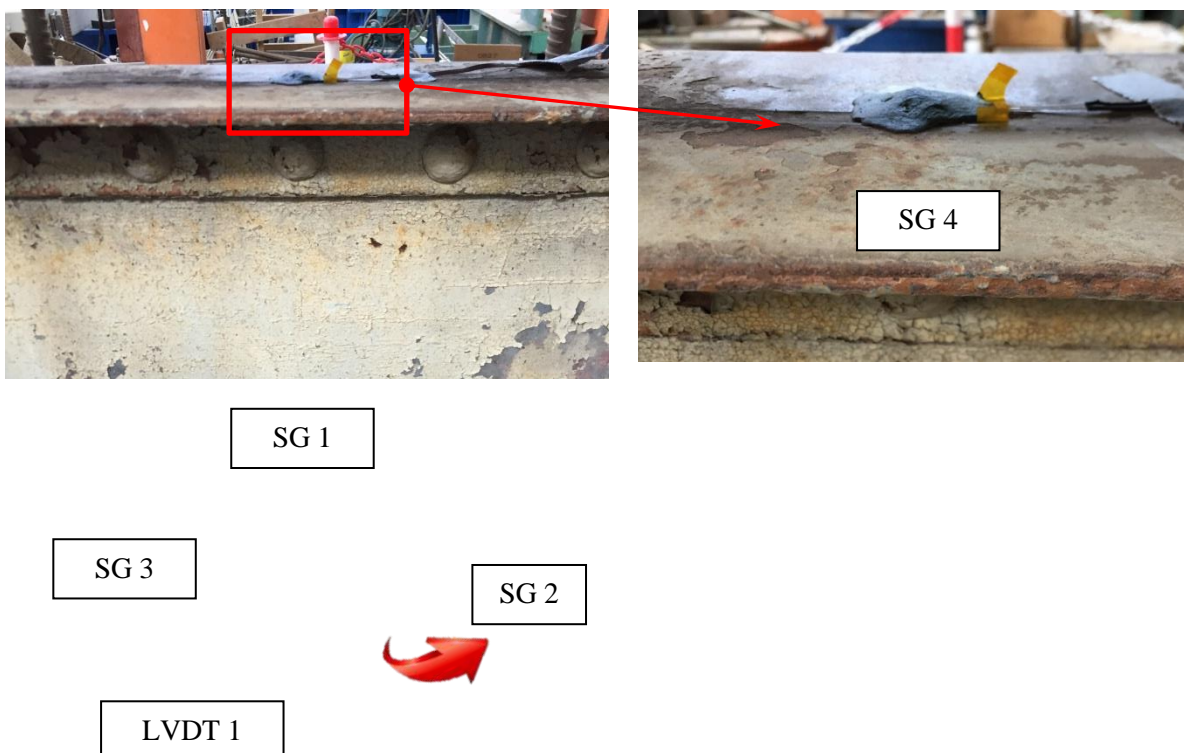




Figure 4: Position of the sensors: strain gauges and Linear variable Displacement Transducers.

189 4.2 Experimental Results

190 The riveted cross beam element can be seen in **Figure 3-a**. **Figure 5** gives the experimental
191 envelopes obtained monitoring strain gauges SG1, SG2, SG3, SG4, and LVDT 1 and LVDT 2.
192 Similarly, **Figure 6** gives the strain increment history obtained by the four strain gauges at the
193 beam mid-span subjected to a constant cyclic load range of 600kN. The strain increment
194 (**Figure 7**) was calculated as the absolute difference between maximum and minimum strains
195 recorded in each cycle. All the sensors monitored similar strain increment trends in four
196 different stages (see **Figure 6**). In the first, there was an initial transitory period of
197 approximately 100 cycles to stabilize the beam's cyclic response, after which the behaviour was
198 stable until approximately the 10000th cycle (stage 2), when a fatigue crack started. At 12k
199 cycles, the strain increment trends abruptly changed due to the rapid propagation of a fatigue
200 crack (stages 3 and 4), which involved a gradual loss of cross beam flexural stiffness and stress
201 redistribution. The strain increments either increased or decreased according to the position of
202 the sensor and the quality of the riveted connection (**Figure 6**).

203 The cross beam failed at approximately 31k cycles. Between cycles 0.1k and 10k, when the
204 behaviour of the cross beam was almost elastic, the strain distribution along the mid-section
205 was not as expected by classic beam theory. According to the literature [2][23][24], the quality
206 of the connections together with high uncertainty plays a crucial role in redistributing the
207 strains in the beam elements. Despite this, the sensors were able to deal with the different
208 stress redistribution as the cracks grew. SG 2 and 3 detected a fatigue crack at an early stage.
209 These sensors monitored varying rates of strain reduction, while, SG1 detected the expected
210 rise of the strain increments (see **Figure 5-a**). This behaviour was caused by the strain
211 redistribution along the element. SG4, on the upper compressed surface, showed a smoother
212 increase of the strain increments than the others (see **Figure 5 -d**). As expected, the SG sensors
213 were all able to warn of the changes in the cross beam's behaviour. Those close to the cracks

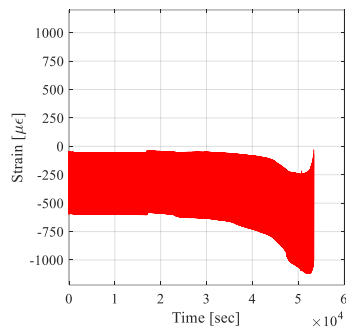
214 (i.e. SG 1, 2 and 3) clearly detected the formation and propagation of cracks at an early stage,
215 while SG 4 was the worst at replicating the spread of the structural failure **(see Figure 5 -a-b-c**
216 **and -d).**

217

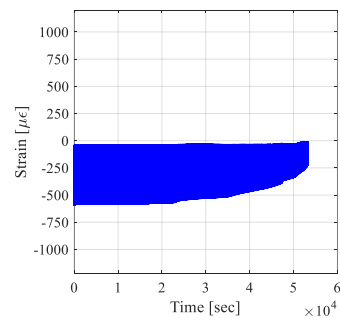
218

219

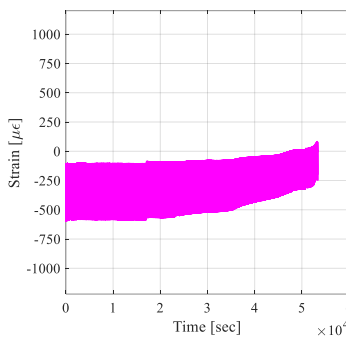
220



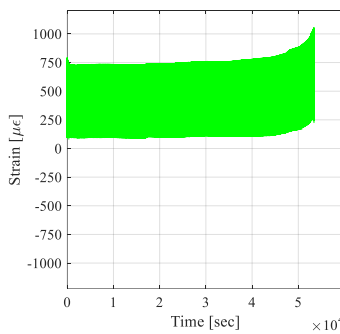
-a



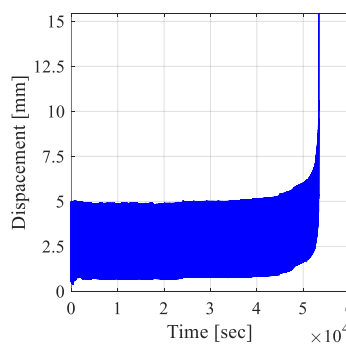
-b



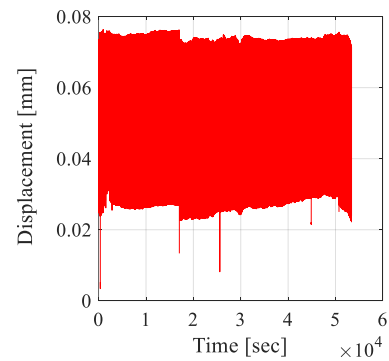
-c



-d



-e



-f

Figure 5: Fatigue test result envelopes: strain gauge SG 1 (-a), SG 2 (-b), SG 3 (-c), SG 4 (-d) (negative strains mean traction) and LVDT1 (-e), LVDT2 (-f).

221

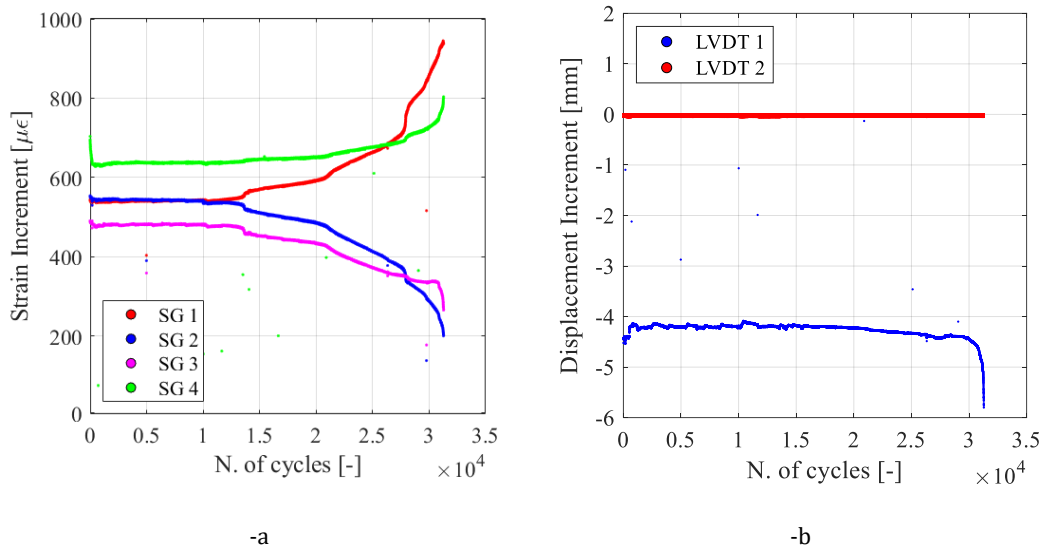


Figure 6: Strain (-a) and displacement (-b) increment histories.

222 A quite different trend was observed in the two LVDTs on the cross beam. LVDT 1 recorded the
 223 vertical displacements in the mid-section and LVDT 2 the possible relative movements at one of
 224 the lateral riveted connections. As can be seen in **Figure 5-e and -f and Figure 6-b**, there were
 225 no relative displacements at the lateral joint, showing that the riveted connection maintained its
 226 integrity. Conversely, LVDT 1 recorded a fairly smooth increase of the mid-span vertical
 227 displacements until approximately 30k cycles, when the cross beam element was about to fail.
 228 Deformation sensors (such as SG) are preferable to displacement sensors because they provide
 229 much more information about the local formation and propagation of fatigue cracks, especially
 230 in elements subjected to bending such as primary girders.

231

232

233

234

235

236

237

238

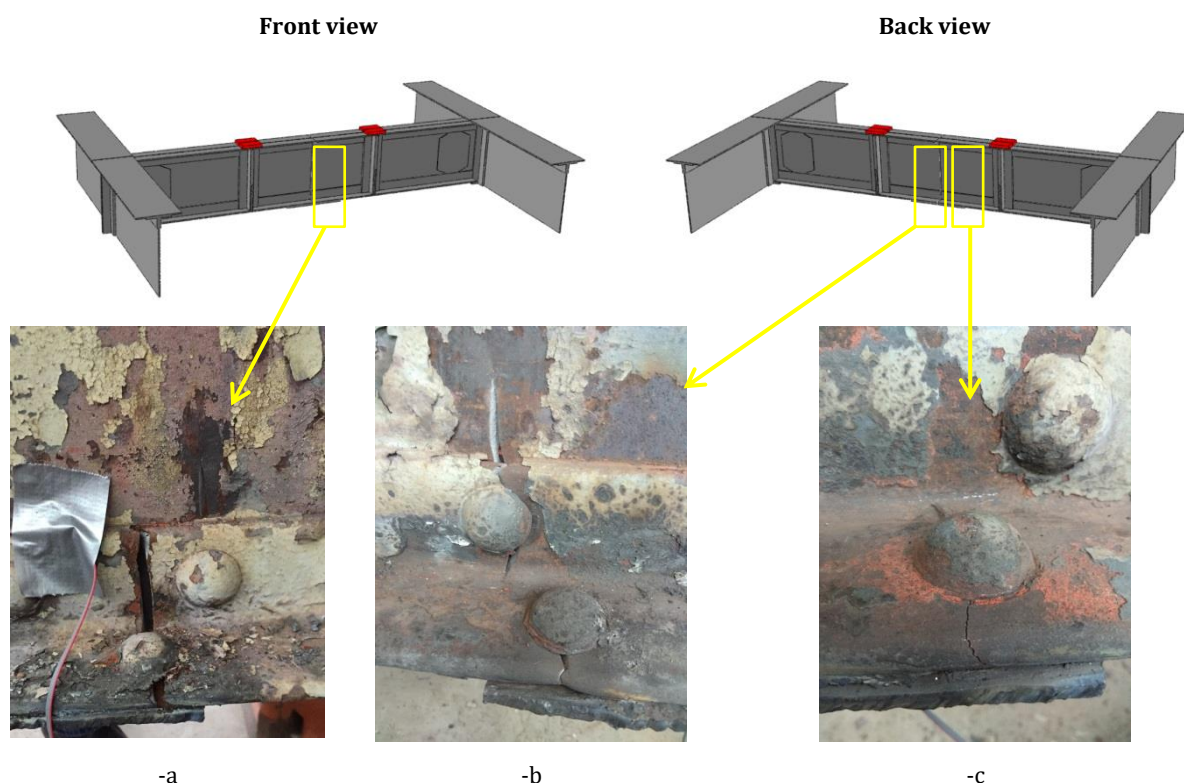


Figure 7: Fatigue cracks observed at the end of the experimental investigation: front (-a) and back (-b) views of first fatigue crack and (-c) back view of the second crack.

240 **Figure 7** shows the crack patterns at the end of the lab test. The cross-beam element has three
 241 similar fatigue cracks at the edges of the cross beam mid-span plate. The mid-span section
 242 comprised one steel plate anchored to the bottom flange which was anchored to the vertical
 243 web. It should be noted that all the joints were riveted. This particular construction technique is
 244 prone to the following issues: (i) a local change of the cross beam flexural stiffness at the ends of
 245 the bottom plate and (ii) a reduction of the bottom flange section due to the presence of rivets.
 246 According to the literature, the most severe cracks begin in the last rivet connecting the bottom
 247 flange to the steel plate, as can be seen in **Figure 7**. The crack then propagated until
 248 compromising the bottom flange and reached the vertical web. **In this case, the different**
 249 **elements composing the girder and connected by rivets were not able to stop the crack**
 250 **propagation.** Indeed, one fatigue crack severely damaged the vertical web in a symmetrical
 251 pattern, which was probably due to the flexural behaviour of the cross beam. During the lab test,
 252 the fatigue crack front propagated from the bottom flanges to the vertical web due to the higher
 253 stresses caused by the progressive drop in the beam's flexural stiffness caused by the damage
 254 itself. It is also interesting to note that another two cracks opened on the opposite plate edge
 255 (see **Figure 7**) but were narrower than the first and did not reach the web.

256 5. Full-scale riveted steel bridge

257 5.1 Fatigue load protocols and experimental set-up

258 A 21 m long isostatic span from the Ferrandet Bridge was moved to the ICITECH laboratories at
259 the *Universitat Politècnica de València* (Spain) (see **Figure 8**). In the laboratory, the bridge was
260 positioned on two hinged and two simple supports (see **Figure 9**). A cyclic load was then
261 applied ranging from 50 to 1300 kN at a frequency of 0.2 Hz (**maximum load and speed of the**
262 **hydraulic jack**) by means of a hydraulic jack positioned vertically over the centre of the span,
263 redistributing the load at four points by means of three stiff beams (green and yellow in **Figure**
264 **9**).



Figure 8: Movement phases: taking from storage area (-a), movement (-b) and laboratory placement (-c).

265 The bridge's structural response was monitored by 40 strain gauges (SG) and 8 Linear Variable
266 Displacement Transducers (LVDTs) collecting data at a sampling rate of 50Hz.

267

268

269

270

271

272

273

274

275

Revised version, modifications highlighted in color **YELLOW**

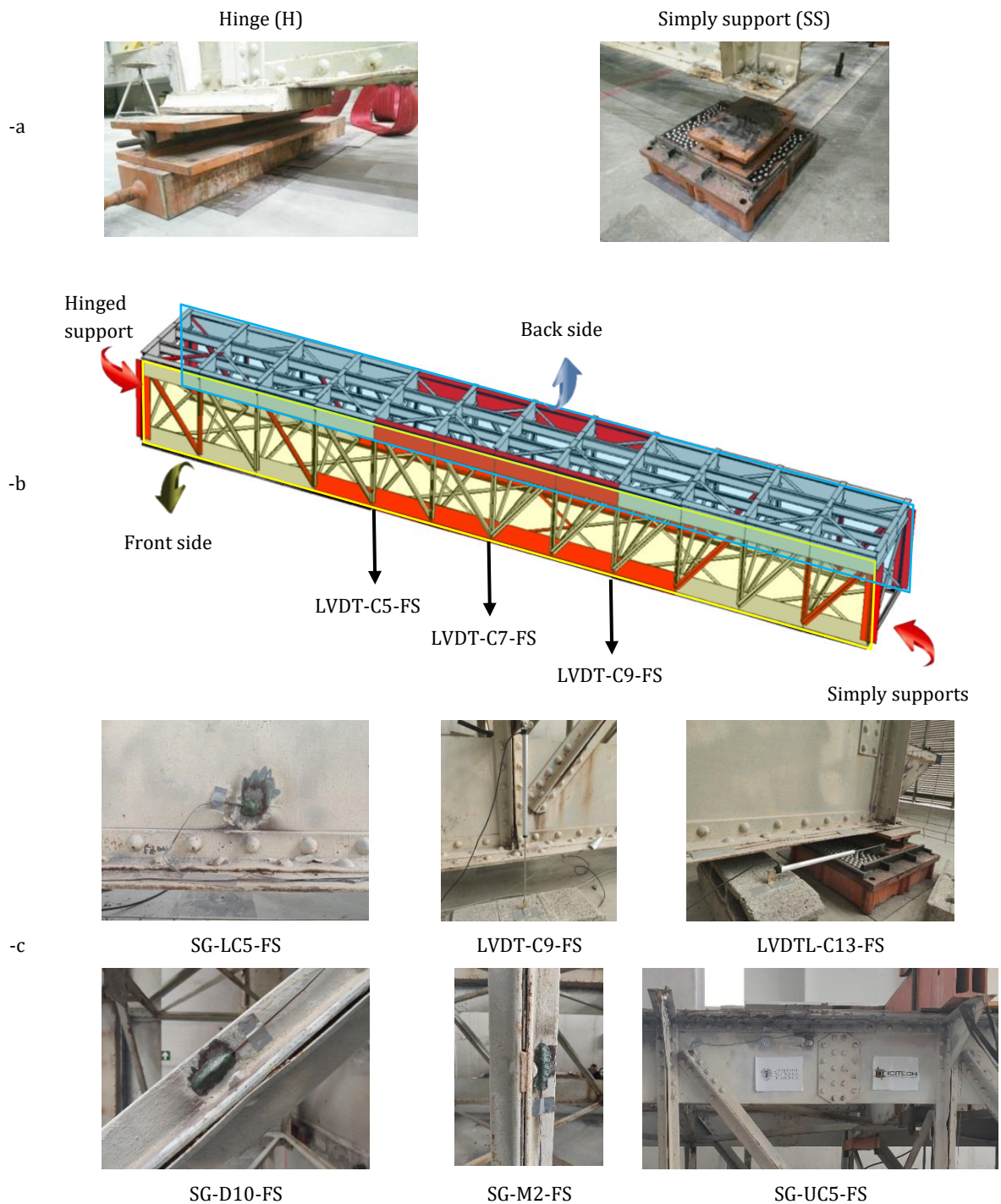


Figure 9: Experimental set-up and sensor network: types of supports (-a), nomenclature details (-b) and types of sensors (-c).

276 The sensor positions are shown in **Figure 9**: (i) position and orientation of the LVDTs (blue
 277 lines) and (ii) structural elements with SGs (red lines), which comprised: upper and lower
 278 central chords, lateral diagonals, vertical truss and upper and lower horizontal bracings. The SG
 279 sensors were placed at the centre of mass of the elements (such as upper and lower chords) and
 280 at the centre **of each element length**. The LVDTs were placed: (i) on the central vertical columns
 281 to monitor the maximum vertical displacements, and (ii) close to the lateral supports to study

282 the transversal and longitudinal movements of the whole structure. The sensor nomenclature
283 followed the general rule: X-YN-Z, where X indicates the sensor type (i.e. SG for strain gauges
284 and LVDT for Linear Variable Displacement Transducers), Y means the element to which the
285 sensor is applied (i.e. C=vertical columns, UP=upper chord, LC=lower chord, D=diagonal,
286 CRV=vertical crux, CRHU=upper horizontal crux and CRHL= lower horizontal crux), N indicates
287 the number of the element starting from the hinged side and Z stands for the position of the
288 element (i.e. FS=front, BS=rear). The horizontal LVDT nomenclature also indicates the sensor
289 orientation (i.e. L and T stand for longitudinal and transversal, respectively).

290 **5.2 Experimental Results**

291 The strain gauge results are depicted in **Figure 10** and include: vertical struts, diagonal
292 elements, upper and lower chords and horizontal bracing. For the sake of brevity, since the
293 fatigue test was over 45k cycles (equivalent to an extra of 27 years more of operational service),
294 only the first and last cycle stress ranges are compared. The calculation of the equivalent
295 number of years was performed considering the strain increment monitored during the
296 laboratory test on the most loaded bottom chord and transforming this value in a stress range
297 (92 MPa) using the elastic modulus of steel. With this stress range, together with the
298 consideration of the real detail category of the structure (see Section 6.3 for more details) and
299 applying the S-N curves methodology, the structure is able to withstand approximately 624k
300 cycles until reaching the collapse of the structure. Since during the lab test 45k cycles were
301 applied to the riveted span, the damage accumulated during the laboratory campaign was equal
302 to approximately 7.2%. Therefore, considering an appropriate behaviour of the structure under
303 fatigue loading until a level of damage of 7.2%, and also taking into account a series of data for
304 the future traffic volume and characteristics (e.g. the maximum real stress of the most loaded
305 bottom chord of the structure is 42.1MPa which is a value monitored in a real field test of the
306 structure, the train passes over the bridge for the future corresponds to the Type 9, 32
307 circulations per day; see Section 6.4 for more details) and the S-N curves methodology, a
308 number of cycles equal to 320k may be withstood by the structure, which could be attained in
309 27 years. The stress ranges were deduced from the strain increments from the sensors and
310 multiplied by the steel Elastic Modulus (210 GPa). In **Figure 10-a** it can be seen that there is a
311 low scatter between the increments in elements C1-FS and C1-BS and on their opposite
312 counterparts C13-FS and C13-BS. Similar findings could be deduced from the results in **Figure**
313 **10-b, -c and -d**, showing almost symmetrical bridge behaviour in both directions. As expected,
314 the stress distribution along the structural elements comprised the central lower chords
315 subjected to higher stress ranges (LC6-FS/BS and LC7-FS/BS). Similarly, higher compressive
316 stresses were obtained in the upper counterparts (UP6-FS/BS and UP7-FS/BS). Diagonals D3-

317 FS/BS and D10-FS/BS were the two subjected to the highest stresses. The shear loads were
 318 higher on the external diagonals and vertical columns, although the stresses were higher in
 319 other elements due to having smaller cross-sections. Three general observations can be made:
 320 (i) the stress level in all the elements is far lower than the elastic limit obtained from the lab
 321 tests reported in Section 3, (ii) none of the elements analysed in the present study obtained
 322 more than a 5% difference between the first and the last cycles; and (iii) visual inspection did
 323 not reveal any damage in the structure.

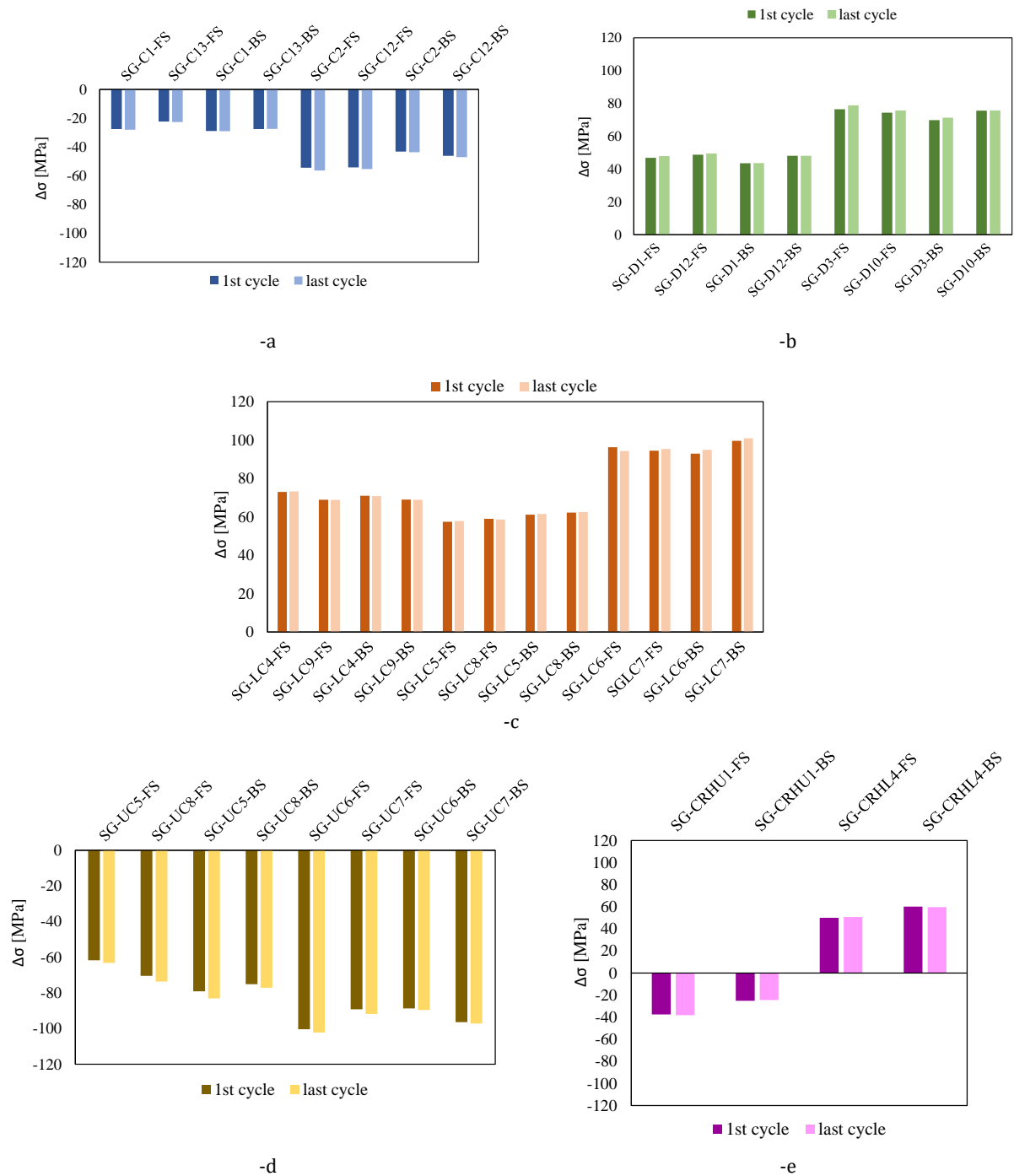


Figure 10: Stress range computed at the beginning and at the end of the test in: (-a) columns, (-b) diagonals, (-c) columns, (-d) columns, (-e) diagonals.

upper chords, (-d) lower chords and (-e) bracing cruxes.

324 **Figure 11** gives the displacement increments read by the LVDTs on the central portion of the
 325 bridge (LVDT-C5-FS/BS, LVDT-C7-FS/BS and LVDT-C9-FS/BS) and those that monitored the
 326 longitudinal and transversal movements of the structure (LVDTL-C13-FS and LVDTT-C13-
 327 FS/BS). As expected, the maximum vertical displacements were observed in the centre of the
 328 bridge. As in **Figure 10**, displacement increments did not vary between the first and last cycle,
 329 again confirming the absence of damage and the elastic behaviour of the bridge. LVDTT-C13-FS
 330 monitored the possible presence of transversal displacement of the support. As shown in
 331 **Figure 11**, there were negligible movements in that direction.

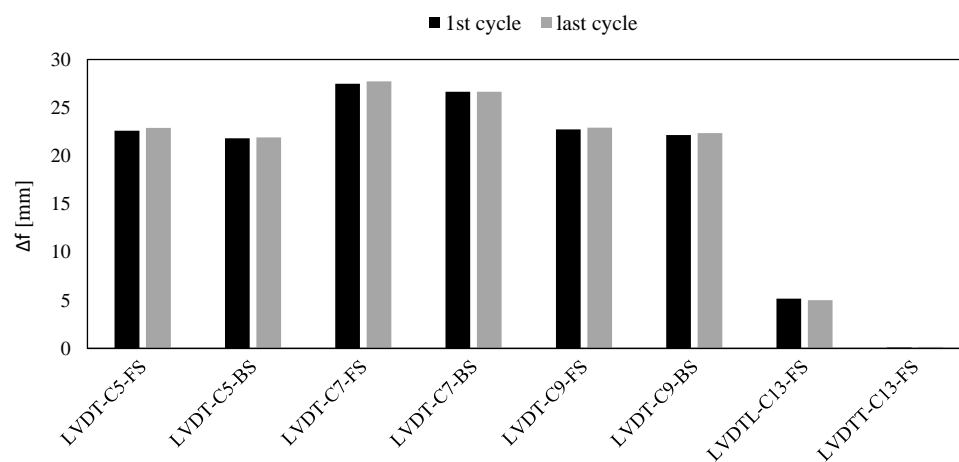
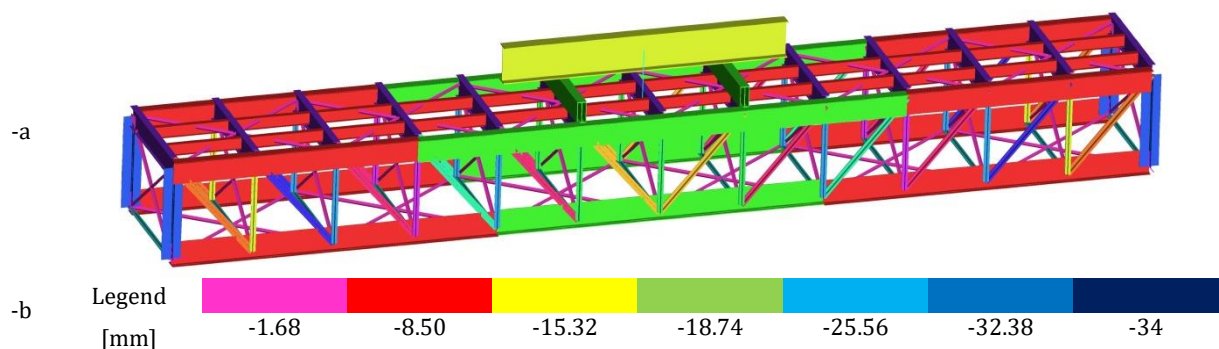


Figure 11: Displacement increment computed at the beginning and at the end of the fatigue test.

332 The experimental results were also compared to the numerical outputs obtained using a 3D
 333 Linear-Static Finite-Element model (LSFE). The isostatic span tested during the lab investigation
 334 was modelled by means of two-noded beam elements, as shown in **Figure 12-a**.

335

336



Revised version, modifications highlighted in color **YELLOW**

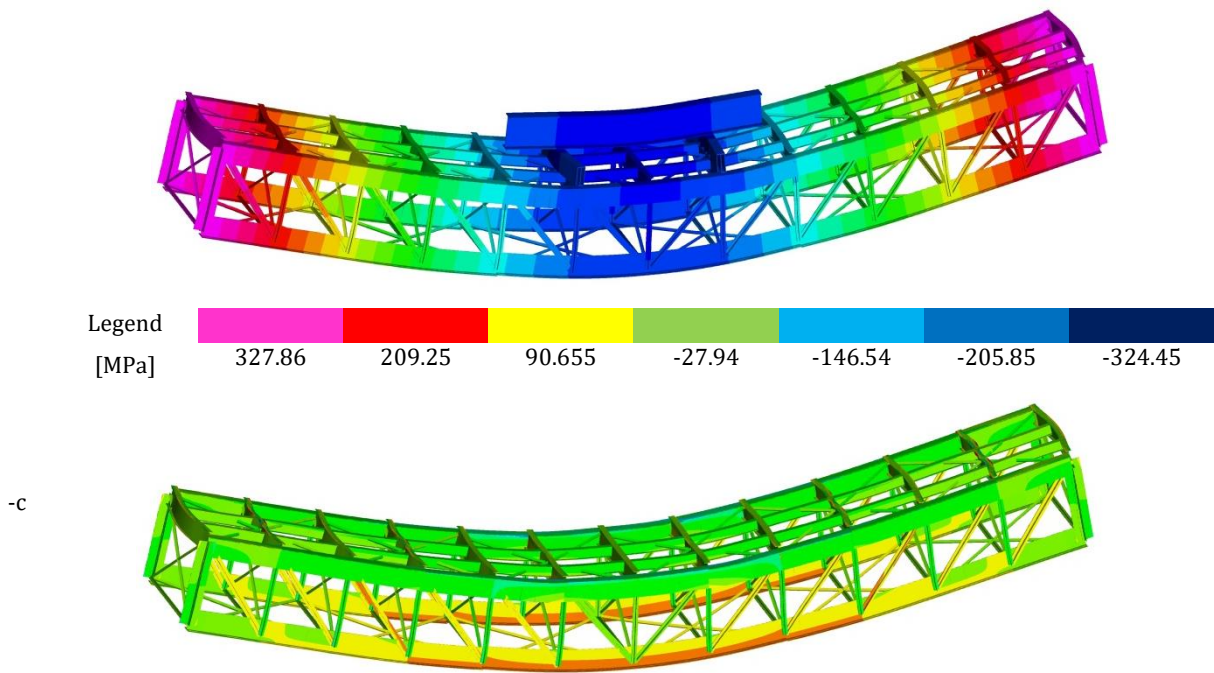


Figure 12: Finite Element model developed to analyse the behaviour of the isostatic span tested during the lab investigation (-a), vertical displacements (negative downwards) (-b) and total stresses along the bridge (-c).

337 **Figure 12-b and -c** gives the vertical displacement and **fibre stresses** produced in the structure
338 by a static load equal to 1250 kN applied on the top of the longitudinal stiff beam. **It is worth**
339 **mentioning that the stresses depicted in Figure 12-c consider both axial stresses and bending**
340 **stresses.** The results slightly overestimated the bridge deformability, with 32 mm of vertical
341 displacement at the centre of the beam, compared with the 27 mm registered by LVDT-C7-
342 FS/BS. A comparison between the experimental and numerical results in terms of total stresses
343 is shown in **Figure 13**. The experimental results given in **Figure 13** were obtained from the
344 average output obtained from each element and their symmetrical counterparts. The model
345 accurately predicted the stress state of each element. The reliability of the model led to its being
346 used for the further analyses described below.

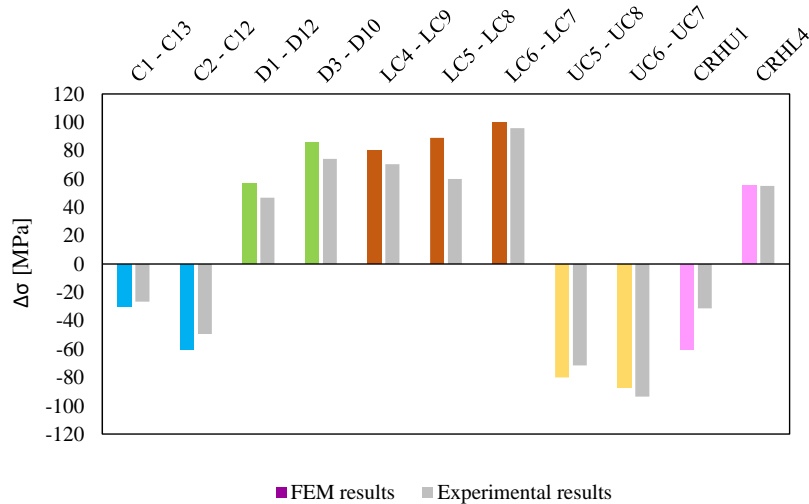


Figure 13: Comparison between experimental (grey bars) and FE results (coloured bars).

347 **6. Analytical evaluation**

348 **6.1 Method**

349 This method was defined for a general case and then applied specifically to the Quisi Bridge. The
 350 analytical assessment following this general method included: (i) load tests on the bridge, (ii)
 351 experimental results from the double experimental tests described in Sections 4 and 5, (iii) the
 352 numerical model validated by the full-scale test outputs, and (iv) the recommendations
 353 proposed by [10]. When all the experimental data is not available, this method also suggests the
 354 criteria to use.

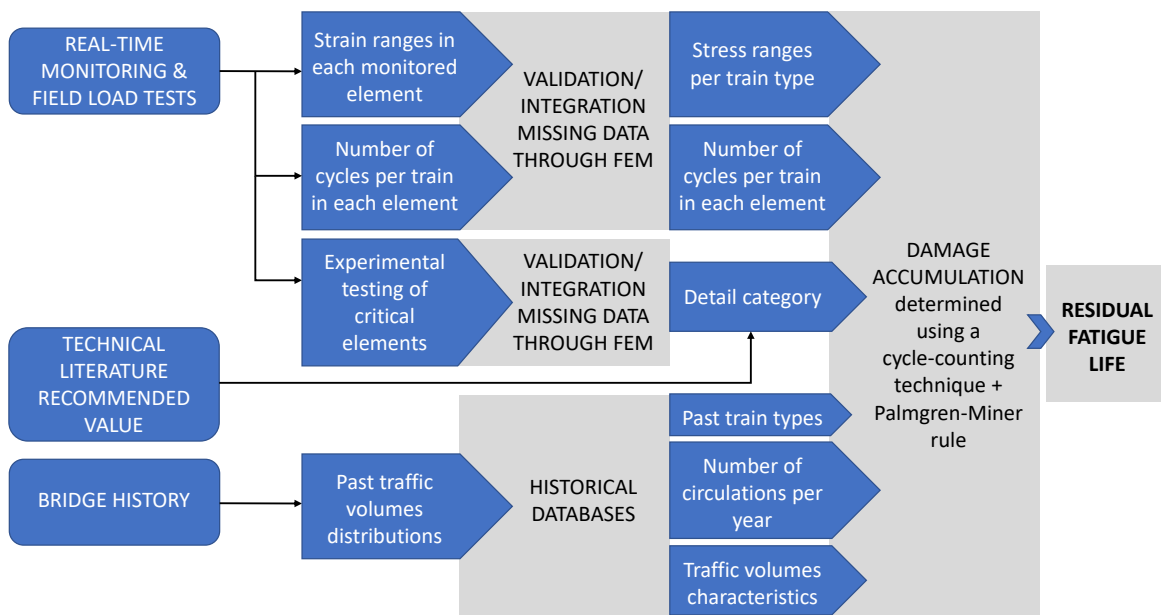


Figure 14: Relational flowchart of the proposed approach.

355

356 The method is organized into five steps **summarized in the relational flowchart depicted in**
357 **Figure 14:**

- 358 1- Collection of information from past traffic volumes considering different train types (see
359 Section 6.2).
- 360 2- Definition of (i) the number of cycles suffered by each element for each train type
361 passing over the bridge and (ii) number of stress-increments in each type of element for
362 a known type of train by real time monitoring during field load tests (see Section 6.2) if
363 available or with the help of numerical simulations.
- 364 3- Extrapolation of stress ranges considering other types of trains and elements and
365 validation throughout numerical simulations (see Sections 6.3 and 6.4).
- 366 4- Definition of detail category, depending on the available data:
- 367 - Adoption of recommended values from [10][11][13], namely: detail category 71 and
368 100, depending on the expected triggered failure mechanism being normal or
369 tangential, respectively.
 - 370 - Through fatigue failure tests of isolated elements such as the one described here and
371 the application of damage accumulation rules such as the Palmgren-Miner rule
372 recommended by EC3 (see Section 6.3).
- 373 5- Estimation of the remaining life of the bridge components applying damage
374 accumulation rules, such as Palmgren-Miner (EC3) and the component's load history.
375 For this, the current accumulated damage of each element is calculated for the
376 subsequent projection of its remaining service life (see Section 6.4).

377 **6.2 Load history and data from field load tests**

378 Rolling loads on bridges such as those produced by vehicles cause variable amplitude stress
379 distributions and typically a large number of cycles. In the broad field of fatigue assessment, the
380 stress distribution can be determined using a cycle-counting technique such as the rainflow
381 counting method. Current standards like the Eurocode 3 [10] for bridge fatigue assessment is
382 based on the Palmgren-Miner rule to account for linear damage accumulation. Although
383 structures with riveted joints are not explicitly referred to in EC3, several experimental
384 investigations have classified these structures as detail category 71 [13]. In the present study,
385 the damage accumulation rule was defined by coupling the stress distribution obtained from
386 field load tests [29] together with the maximum stresses obtained in the elements of a 3D LSFE

387 model of the whole bridge. The field tests on the Quisi Bridge were used to estimate its dynamic
388 behaviour under the load of a specific train type (Train 9) [29].

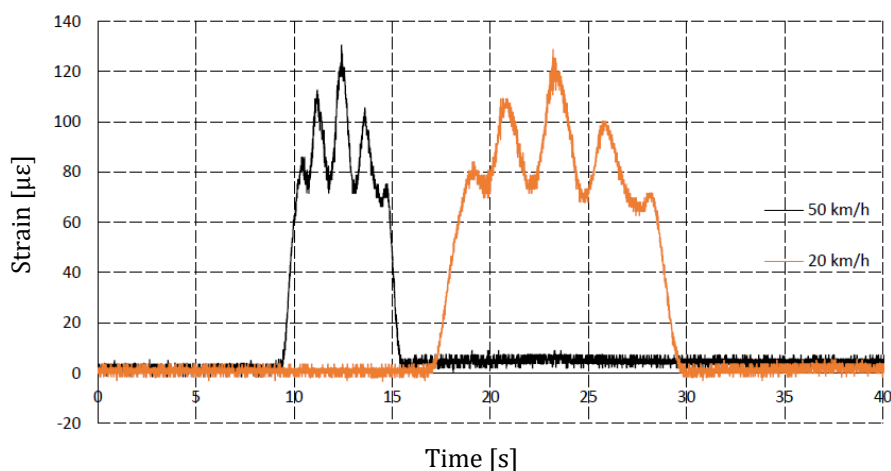


Figure 15: Strain distribution caused by the circulation of train 2500 in the central lower chord (isostatic span) assuming two different train velocities. Source: Ivorra et al. [29].

389 **Figure 15** gives the strain distribution monitored in the central lower chord of one of the
390 isostatic spans. The measurements were taken at two different train speeds. **Figure 15** shows
391 that the speed did not affect the maximum strain or the number of cycles obtained in the lower
392 chord. The strain distribution of the most representative elements was compared to the
393 numerical output obtained from a static analysis. The results of the field tests were used to
394 evaluate: (i) cyclic stress characteristics associated with the different train loads. These results
395 showed that cross-beams and stringers (longitudinal primary beams) are subjected to one cycle
396 per axle, while all the other elements are subjected **to** lower cycles (cycles per train); (ii) the
397 dynamic effect of train loads and the **stress ranges** in all the elements (the latter was deduced
398 from the LSFE model). Deformation was found to increase by 30% **in the field tests with respect**
399 **to the FE analysis**, resulting in a dynamic amplification factor of 1.3. The bridge's detail class
400 was calculated from the information available on its loading history in service expressed by
401 traffic volumes and their characteristics (**see more details in Section 6.3**). Assuming a period
402 dating from 1915 to the present, 11 different types of train passed over the bridge, as can be
403 seen in **Figure 16**.

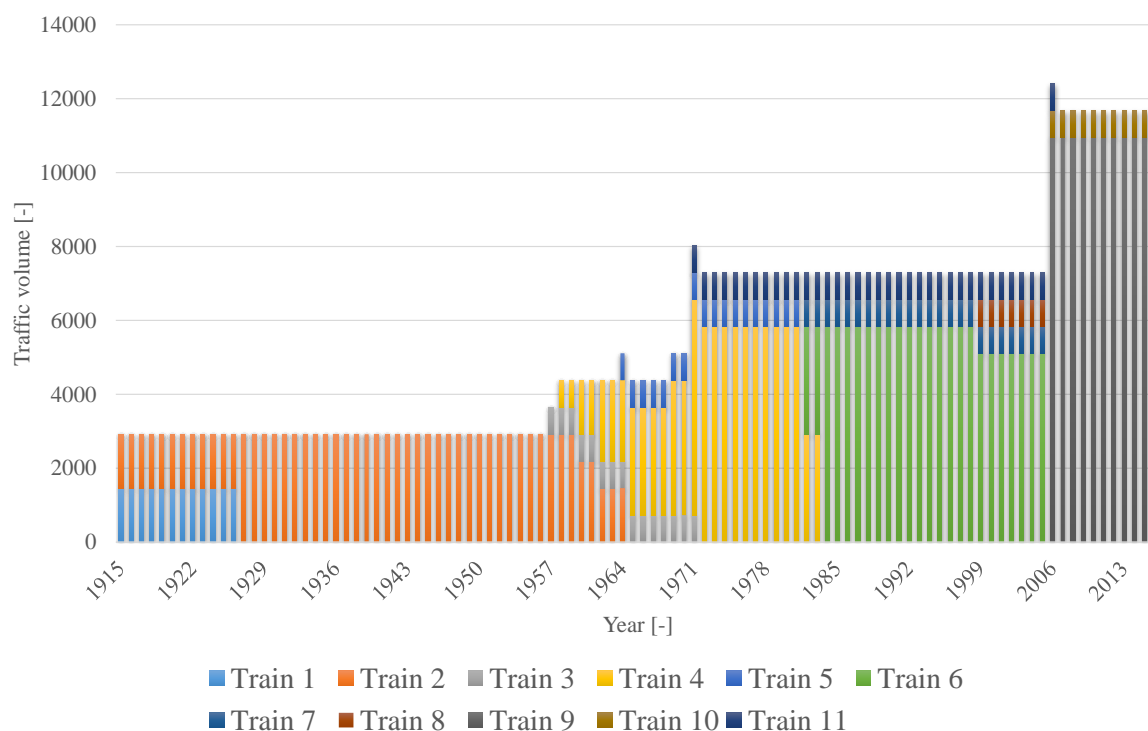


Figure 16: Loading history of the bridges during their exploitation expressed by train typology distributions over the years and traffic volumes. Data provided by the railway administration.

404 6.3 Definition of detail category based on test results

405 This section describes the calculation of the detail class of the cross beam from the experimental
 406 results described in Section 4, the information available on traffic volumes and the Eurocode 3
 407 recommendations. The cross beam detail class was obtained assuming two different
 408 hypotheses: (i) trains were either completely loaded or (ii) only 80% loaded (this load is
 409 approximately the self-weight of the different train types). These two assumptions were made
 410 to take into account the uncertainty of the historical traffic loads. **Past damage accumulation**
 411 **was deduced from the traffic volumes reported in Figure 16 considering that the cross beam**
 412 **was 100% damaged during the lab test (i.e. after 31,377 cycles) and following the Palmgren-**
 413 **Miner rule. In detail, the total damage accumulation was divided into two parts: (i) damage**
 414 **accumulated during past train circulations and (ii) residual damage needed to reach the failure**
 415 **of the structure (100% damage as it was damaged during the lab test). In the first part, the**
 416 **accumulated damage was estimated as a function of the detail category (still unknown) and**
 417 **based on typical strain distribution patterns obtained in critical cross beams during field load**
 418 **tests. The information obtained during the real time field load tests allowed the calculation of**
 419 **the number of cycles per train passage and the strain increment associated with each**
 420 **circulation. In the second part, the number of cycles and the stress ranges applied to the**
 421 **element during the laboratory test were used to calculate the total damage of the cross beam as**

Revised version, modifications highlighted in color **YELLOW**

422 a function of the detail category. It is worth mentioning that the procedure adopted included a
423 first hypothesis of the detail category which was then estimated by verifying that the complete
424 damage (damage 100%) had been obtained after the laboratory test. In the 100% and 80%
425 loading scenarios detail classes of 71 and 63 were deduced, respectively. The results, in terms of
426 accumulated damage during consecutive periods of bridge operation from 1915 (blue bars) and
427 the lab test (red bar) are given in **Figure 17-a and -b** and confirm that the cross beam would
428 fail at detail category 71, for fully loaded trains, and at detail category 63 for 80% loaded trains.

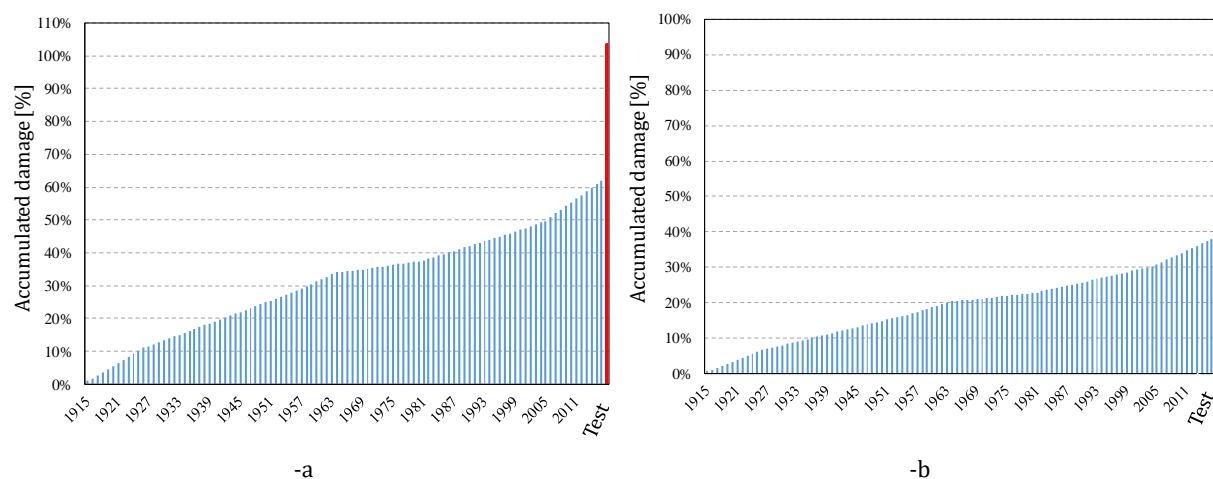


Figure 17: Accumulated damage distributions over the bridges exploitation, considering: trains loaded at 100% (-a) and at 80% (-b).

429 **6.4 Estimation of the remaining fatigue life**

430 Remaining fatigue life can be analysed using LSFE models for stress amplitudes and the number
431 of cycles undergone by each element. The Quisi Bridge was analysed adopting the LSFE model
432 described above (see **Figure 18**). **Table 5** shows the results obtained for future traffic loads
433 over the bridge (Train Type 9) without considering a dynamic amplification factor. **In detail,**
434 **strain increment patterns due to train circulation obtained from field load tests were used**
435 **together with FE outputs to estimate the number of cycles per train circulation and the**
436 **maximum stress ranges in the most critical elements composing the structure. This information**
437 **was used to extrapolate the damage accumulated from 1915 till 2016.**



Figure 18: Finite Element model of the whole bridge, considering the strengthening and reparations introduced in the structure.

Structural Element		Maximum stress [MPa]
Lower chord		32.4
Diagonal		29.7
Cross beam	Axle 1	32.8
	Axle 2	28.6
Stringer	Axle 1	14.8
	Axle 2	12.9

439 It is important to remember that, in this case, cross beams and stringers are directly subjected
 440 to the cycles produced by each axle, instead of 3 cycles per train, and therefore to higher
 441 accumulated damage than other elements. Considering a detail class equal to 71 or 63 for fully
 442 or 80% loaded trains, respectively (computation was performed in this case with detail class 63
 443 but results are identical in both situations), assuming that the expected traffic volume in the
 444 next 10 years will consist of 32 type 9 trains **per day** and using the S-N curves method
 445 recommended by Eurocode 3, the damage caused in this period can be extrapolated.

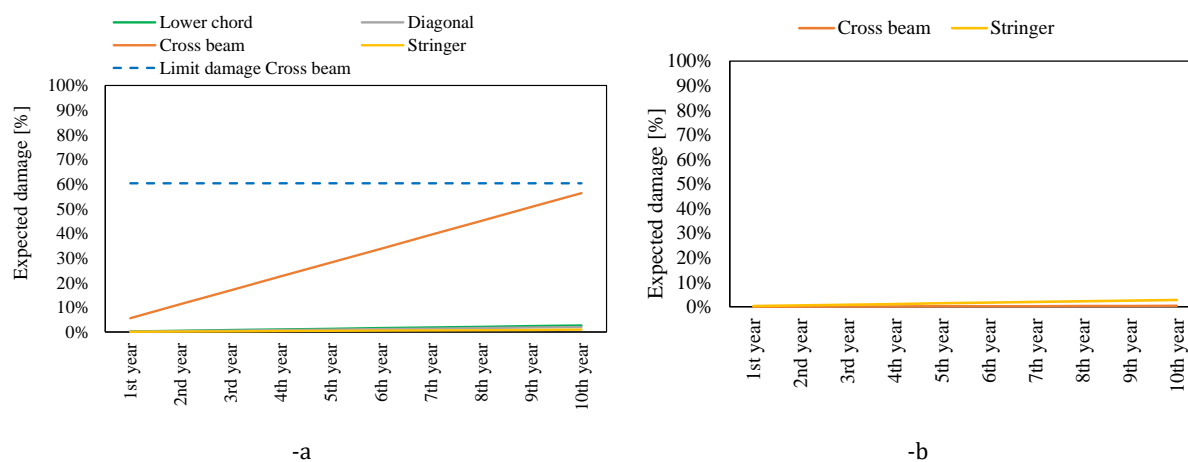


Figure 19: Expected accumulated damage in different structural elements considering: normal stresses (-a) and tangential stresses (-b).

446 **Figure 19-a** gives the damage percentages (due to normal stresses) expected to be accumulated
 447 in future train passages. This information must be coupled with the results illustrated in **Figure**
 448 **17-b** which shows the percentages of past damage accumulated by the bridge during
 449 operational service using the detail category of 63 and 80% of the loaded trains. From that data
 450 it is possible to see that, before the laboratory test, the bridge accumulated (from 1915 to 2016)
 451 about 40% of damage. In the next 10 years, the cross beams will reach the 60% damage limit
 452 available considering a detail class 63 and 80% loaded train (Section 6.2), according to the
 453 information in **Figure 19-a**. The same calculation was repeated considering the tangential

454 stresses in the riveted connections taking into account the number of rivets composing the
455 lateral connections of each element and the cross-section of each rivet. The results are given in
456 **Figure 19-b** considering only cross beams and stringers and the lower detail class
457 recommended by Eurocode 3 (80, the lowest in EC3). As can be seen in **Figure 19-b**, the damage
458 expected in the next 10 years due to tangential stresses is quite low. Results from **Figure 19 -a**
459 **and -b** confirm that the cross beams are the most vulnerable elements in the bridge (**Figure 19**
460 **-a**) and that normal stresses will be responsible for future fatigue damage (**Figure 19 -a and -**
461 **b**).

462 7. Conclusions

463 This paper describes a study that aimed to provide meaningful experimental results on the
464 fatigue behaviour of riveted steel railway bridges subjected to rolling loads in a combination of:
465 (i) an ambitious experimental study with two full-scale tests to study local and overall bridge
466 fatigue performance; and (ii) an analytical evaluation to assess the bridge's remaining fatigue
467 life. The study was carried out on two riveted steel bridges in the Valencia railway network: the
468 Quisi and Ferrandet Bridges, from which the following conclusions can be drawn:

- 469 - A cross beam element was subjected to a 0.55 Hz frequency cyclic load ranging from 50
470 to 650 kN to assess the local behaviour of the structure. The results showed that:
 - 471 ○ Fatigue cracks most probably nucleated after 10 k cycles and progressed fairly
472 quickly until collapse at approximately 31k cycles.
 - 473 ○ The LVDT that monitored maximum vertical displacements was unable to
474 capture any warning signs of imminent failure before 30k cycles, while strain
475 gauges on the central section were able to track the redistribution of stresses as
476 the cracks grew.
 - 477 ○ A fatigue test on a cross beam showed that fatigue cracks are likely to appear
478 near to the central section. This finding could be explained by the peculiar
479 geometry of the element and by the presence of an additional lower plate
480 responsible for a sudden change in flexural stiffness.
 - 481 ○ Estimation of the detail class using the traditional S-N curves method found
482 cross beam detail classes of between 63 and 71, depending on the uncertainties
483 related to traffic loads.
- 484 - A full-scale fatigue test of an isostatic span was carried out to assess the structure's
485 overall behaviour and reached the following conclusions:
 - 486 ○ The test identified the most heavily loaded elements and furnished the
487 experimental results to calibrate a Finite Element model.

- 488 ○ The fatigue test lasted for 45k cycles with a **load range** equal to 1250kN. During
489 the lab investigation, the steel span showed elastic behaviour without the
490 appearance of any fatigue damage. This confirmed that the non-primary
491 elements of the bridge could be expected to operate safely for 27 more years.
- 492 - An analytical method based on load tests, numerical modelling, recommendations and
493 codes was **adopted** to evaluate remaining bridge fatigue life. Its application to the bridge
494 under study reached the following conclusion:
- 495 ○ Fatigue calculations of the Quisi Bridge's remaining fatigue life identified the
496 cross beams as the most vulnerable elements. Fatigue failures can be expected to
497 arise in the next 10 years due to normal stresses, but not in the lateral riveted
498 connections.

499 **This work represents a step toward understanding the overall and local fatigue responses of old**
500 **riveted steel bridges with a unique double experimental investigation. The results are expected**
501 **to increase the existing fatigue test database: (i) confirmation of the detail category of steel**
502 **riveted structures and (ii) the adoption of an analytical method applicable to other cases. A**
503 **possible future extension of the present research line is represented by the evaluation of a**
504 **wider number of critical principal elements (i.e. transversal girder and stringers) subjected to**
505 **variable amplitude stress ranges, such as those produced in highway bridges.**

506

507 **8. Acknowledgements**

508 The authors would like to express their gratitude to the FGV (*Ferrocarrils de la Generalitat*
509 *Valenciana*) and *FCC Construcción S.A.*, *CHM Obras e Infraestructuras S.A.*, *Contratas y Ventas S.A.*
510 and *CALSENS S.L.* for giving us the opportunity to test a bridge at the ICITECH facilities, also to
511 Juan Antonio García Cerezo, of *FGV*, for his invaluable cooperation and recommendations. We
512 also wish to show our gratitude for the magnificent work on the bridge by Eduardo Luengo,
513 Salvador Ivorra, Juan J. Moragues, Benjamín Torres, Daniel Tasquer and Jesús Martínez. The
514 tests on the bridge meant that much of the Structures Laboratory was out of service for other
515 work, for which we owe a debt of gratitude to our *ICITECH* colleagues for their infinite patience
516 and understanding.

517

518 **9. References**

- 519 [1] M. Kuźawa, T. Kamiński, J. Bień, Fatigue assessment procedure for old riveted road
520 bridges, *Archives of Civil and Mechanical Engineering*, v 18- 4, 2018, pp 1259-1274.

- 521 [2] B. Pedrosa, J. A. F. O. Correia, C. Rebelo, G. Lesiuk, M. Veljkovic, Fatigue resistance curves
522 for single and double shear riveted joints from old portuguese metallic bridges,
523 Engineering Failure Analysis,v 96, 2019, pp 255-273.
- 524 [3] L. Sieber, R. Urbanek, J. Bär, Crack-Detection in old riveted steel bridge structures,
525 Procedia Structural Integrity,v 17, 2019, pp 339-346.
- 526 [4] A.M.P. De Jesus, A.L.L. da Silva, M.V. Figueiredo, J.A.F.O. Correia, A.S. Ribeiro, A.A.
527 Fernandes, Strain-life and crack propagation fatigue data from several Portuguese old
528 metallic riveted bridges, Eng. Fail. Anal., v 18-1, 2011, pp. 148-163.
- 529 [5] D. Leonetti, J.Maljaars, G. Pasquarelli, G. Brando, Rivet clamping force of as-built hot-
530 riveted connections in steel bridges, Journal of Constructional Steel, v 167, 2020;
- 531 [6] D. Leonetti, J.Maljaars, H. H. Snijder, Fatigue life prediction of hot-riveted shear
532 connections using system reliability, Engineering Structures,v 1861, 2019, pp 471-483.
- 533 [7] H. Heydarinouri, A. Nussbaumer, J. Maljaars, E. Ghafoori, Proposed criterion for fatigue
534 strengthening of riveted bridge girders, Procedia Structural Integrity,v 19, 2019, pp 482-
535 493.
- 536 [8] Z. Liu, M. Hebdon, J. Correia, H. Carvalho, P. Vilela, A. De Jesus, R. Calçada, Fatigue
537 assessment of critical connections in a historic Eyebar suspension bridge, J. Perform.
538 Constr. Facil., v 33-1, 2019.
- 539 [9] A. Taras, R. Greiner, Development and application of a fatigue class catalogue for riveted
540 bridge components, Struct. Eng. Int., v 20-1, 2010, pp. 91-103.
- 541 [10] CEN, EN 1993-1-9: Eurocode 3, Design of Steel Structures – Part 1–9: Fatigue,
542 European Committee for Standardization, Brussels (2005).
- 543 [11] American Association of State Highway and Transportation Officials (AASHTO),
544 Guide Specifications for Fatigue Evaluation of Existing Steel Bridges, Washington, D.C.,
545 (1990).
- 546 [12] American Railway Engineering and Maintenance of way Association (AREMA),
547 Manual for Railway Engineering, (2019).
- 548 [13] B. Kühn, M. Lukic, A.Nussbaumer, H.P.Günther, R. Helmerich, S.Herion,
549 M.H.Kolstein, S. Walbridge, B.Androic, O. Dijkstra, and Ö. Bucak, Assessment of existing
550 steel structures: Recommendations for estimation of the remaining fatigue life. EUR -
551 Scientific and Technical Research Series, Luxembourg, 2008.
- 552 [14] A. Cunha, E. Caetano, F. Magalhães, C. Moutinho, Recent perspectives in dynamic
553 testing and monitoring of bridges, J Struct Control Health Monit, v 20-6, 2012, pp 853-
554 877.

- 555 [15] F. Magalhães, A. Cunha, E. Caetano, Vibration based structural health monitoring
556 of an arch bridge: from automated OMA to damage detection, *MechSyst Signal Process*, v
557 28, 2012, pp 212-228.
- 558 [16] J. Leander, A. Andersson, R. Karoumi, Monitoring and enhanced fatigue
559 evaluation of a steel railway bridge, *EngStruct*, v 32, 2010, pp 854-863.
- 560 [17] B. Caglayan, K. Ozakgul, O. Tezer, Fatigue life evaluation of a through-girder steel
561 railway bridge, *Eng Failure Anal*, v 16-3, 2009.
- 562 [18] B. M. Imam, T. D. Righiniotis, M. K. Chryssanthopoulos, Numerical modelling of
563 riveted railway bridge connections for fatigue evaluation, *Engineering Structures*, v 29-
564 11, 2007, pp 3071-3081.
- 565 [19] A.H. DePiero, R.K. Paasch, S.C. Lovejoy, Finite-element modelling of bridge deck
566 connection details, *J Bridge Eng (ASCE)*, v 7-4, 2002, pp 229-235.
- 567 [20] M. Al-Emrani, R. Kliger, FE analysis of stringer-to-floor-beam connections in
568 riveted railway bridges, *J Constr Steel Res*, v 59-7, 2003, pp 803-818.
- 569 [21] M. Al-Emrani, Fatigue performance of stringer-to-floor-beam connections in
570 riveted railway bridges, *J Bridge Eng (ASCE)*, v 10-2, 2005, pp 179-185.
- 571 [22] J. Tulonen, T.Siitonen, A. Laaksonen, Behaviour of riveted stringer-to-floorbeam
572 connections in cyclic load tests to failure, *Journal of Constructional Steel Research*, v
573 160, 2019, pp 101-109.
- 574 [23] A. Pipinato, M. Molinari, C. Pellegrino, O. S. Bursi, C. Modena, Fatigue tests on
575 riveted steel elements taken from a railway bridge, *Struct. Infrastruct. Eng.*, v 7-12, 2009,
576 pp 907-920.
- 577 [24] A. Pipinato, C. Pellegrino, O. S. Bursi, C. Modena, High-cycle fatigue behavior of
578 riveted connections for railway metal bridges, *J. Constr. Steel Res.*, v 65, 2009, pp 2167-
579 2175.
- 580 [25] A. De Jesus, M. Figueiredo, A. Ribeiro, P. Castro, A. Fernandes, Residual lifetime
581 assessment of an ancient riveted steel road bridge, *Strain*, v 47-1, 2011, pp 402-415.
- 582 [26] A. Azizinamini, "Full scale testing of old steel truss bridge." *Journal of*
583 *Constructional Steel Research*, v. 58-5-8, 2002, pp 843-858.
- 584 [27] UNE EN ISO 6892-1:2017: Metallic materials - Tensile testing - Part 1: Method of
585 test at room temperature (ISO 6892-1:2016).
- 586 [28] UNE EN ISO 148-1:2017: Metallic materials - Charpy pendulum impact test - Part
587 1: Test method (ISO 148-1:2016).
- 588 [29] S. Ivorra, M. Buitrago, E. Bertolesi, B. Torres, and D. Bru, Dynamic identification
589 on an ancient steel bridge of six spans, 14th International Workshop on Advanced Smart

Revised version, modifications highlighted in color **YELLOW**

590 Materials and Smart Structures Technology (ANCRiSST), V. Gattulli, O. Bursi, and D.
591 Zonta, eds., Sapienza. Università Editrice, Rome, 139–142, 2019.